Generalized MIMO Transmit Preprocessing Using Pilot Symbol Assisted Rateless Codes

Nicholas Bonello, Du Yang, Sheng Chen and Lajos Hanzo
School of ECS, University of Southampton, SO17 1BJ, United Kingdom.
Email: {nb06r,dy05r,sqc,lh}@ecs.soton.ac.uk, http://www-mobile.ecs.soton.ac.uk

***Abstract*— In this paper, we propose a generalized multiple-input multiple-output (MIMO) transmit preprocessing system, where both the channel coding and the linear MIMO transmit precoding components exploit the knowledge of the channel. Moreover, we also propose a novel technique, hereby referred to as pilot symbol assisted rateless (PSAR) coding, where a predetermined fraction of binary pilot symbols is interspersed with the channel-coded bits at the channel coding stage, instead of multiplexing the pilots with the data symbols at the modulation stage, as in classic pilot symbol assisted modulation (PSAM). We will subsequently demonstrate that the PSAR code-aided transmit preprocessing scheme succeeds in gleaning more beneficial knowledge from the inserted pilots, because the pilot bits are not only useful for estimating the channel at the receiver, but they are also beneficial in terms of significantly reducing the computational complexity of the rateless channel decoder.**

I. Introduction

One of the most significant technological breakthroughs of contemporary wireless communications is constituted by multiple-input multiple-output (MIMO) transceivers, which provide an elegant solution for further extending the channel's capacity limits and for enhancing the link reliabilities. More pronounced efficiency gains can be expected if both the transmitter and receiver are capable of exploiting channel state information (CSI). In such systems, the CSI at the receiver (CSIR) is typically obtained by estimating the unknown channel parameters based on known pilot bits, and then this information is fed back to the transmitter on a feedback channel. Furthermore, the CSI at the transmitter (CSIT) is usually exploited by a technique that is commonly referred to as transmit preprocessing [1]. This configuration consists of two separate components; a predetermined (i.e. fixed-rate), CSIT-independent channel coding scheme amalgamated with a linear CSIT-dependent MIMO transmit precoder. In this paper we are advocating a solution, where **both** the channel coding as well as well as the linear MIMO transmit precoder components exploit the knowledge of CSIT. We argue that since the scheme of [1] already received CSIT with the aid of a readily available feedback channel from the receiver, then providing CSIT information not only for the MIMO precoder but also for the channel encoder does not impose substantial complications.

The first modification that has to be carried out for the system of [1], is that the channel code to be employed can now no longer have predetermined constraints, such as that of having a fixed-rate and a rigid construction, but has to additionally rely on online processing techniques for exploiting the available CSIT, in a similar manner to that of the linear MIMO transmit precoder. The second modification that we impose is related to the degree distribution employed by these rateless codes. In [2], we have studied the degree distribution of a rateless code, analyzed the optimum distribution across a diverse range of channel signal-to-noise ratio (SNRs) and demonstrated that there are substantial differences between these distributions. Consequently, it was argued that rateless codes having a fixed degree distribution are sub-optimal in the sense that they cannot realize codes that operate near to capacity at all possible rates. However, in the specific scenario we are considering here, the rateless encoder is armed with side information and therefore it is capable of calculating, in a near-realtime online manner, the specific degree distribution that results in a performance that is arbitrarily close to capacity.

The financial support of both the EPSRC U.K., and that of the EU under the auspices of the Optimix project is gratefully acknowledged.

Another contribution of this paper is related to the channel estimation to be used at the receiver for determining the CSIR. There are mainly two approaches that are frequently employed to estimate the channel; namely that of either estimating the channel blindly or using reference/pilot symbols. For all intents and purposes of this paper, the downlink (DL) receiver of the mobile station (MS) estimates the channel's amplitude and phase using known pilots and then conveys this CSI estimate back to the DL transmitter of the base station (BS). However, instead of inserting pilots at the modulation stage as in classic PSAM, we propose a novel rateless code, termed as the pilot symbol assisted rateless (PSAR) code, that appropriately intersperses a predetermined fraction of pilot bits along with the codeword bits. The motivation behind using PSAR codes is that of gleaning more information from the pilot overhead "investment", than just simply the capability of channel estimation such as in the PSAM technique.

II. Channel Model

We consider a single-user MIMO system employing two transmit and two receive antennas. The canonical continuous-time complex baseband-equivalent MIMO channel model used is given by $\mathbf{y}(t) = \mathbf{H}(t)\mathbf{x}(t) + \mathbf{n}(t)$, where $\mathbf{x}(t)$, $\mathbf{y}(t) \in \mathbb{C}$ are vectors corresponding to the transmitted and received signals of the respective antennas. The time-variant MIMO channel matrix $\mathbf{H}(t)$ contains elements corresponding to the channel gains of a Rayleigh-fading process generated according to a complex circularly symmetric Gaussian distribution and with an autocorrelation function $r_{aa}(\tau)$ formulated by $r_{aa}(\tau) = J_0(2\pi \overline{f}_m \tau)$, where τ represents the correlation lag, $J_0(\cdot)$ represents the zero-order Bessel function of the first kind and $\overline{f}_m$ is the normalized Doppler frequency. The complex additive white Gaussian noise (AWGN) is represented by the vector $\mathbf{n}(t) \sim \mathcal{CN}(0, N_0)$, where N_0 denotes the two-dimensional noise variance. The near-instantaneous SNR encountered at the receiver antenna i, $\overline{\psi}_i$, and associated with a particular channel realization $\mathbf{h}_i(t) = [h_{i,1}\ h_{i,2}]$ is then given by $\overline{\psi}_i := E_s|\mathbf{h}_i(t)|^2/2\sigma_n^2$, where E_s and $|\mathbf{H}(t)|^2$ represent the constant energy-per-symbol at a specific antenna and the fading power coefficients, respectively. The average SNR at the receiver is then given by $\psi_{i,\text{avg}} := \left[E_s\mathcal{E}(|\mathbf{h}_i(t)|^2)\right]/N_0$, where $\mathcal{E}(\cdot)$ denotes the expectation operator. Since the statistical distribution of the channel realizations between any two pair of transmit and receive antennas is identical, then the average SNR at each antenna is also identical. Consequently, we will simply use the MIMO system's SNR, denoted here by ψ_{avg}.

III. System Model

Figure 1 illustrates a top-level schematic of the proposed system model. For the sake of simplifying our analysis, we will refer to the two CSI-assisted components in the system as the inner

978-1-4244-2519-8/10/$26.00 ©2010 IEEE

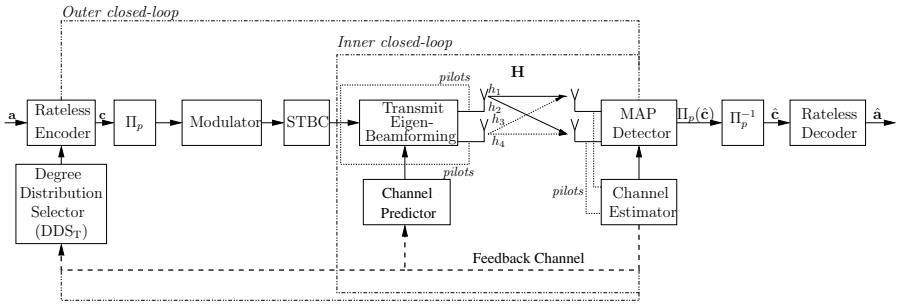

Fig. 1. The generic system model, having two components of the system that are exploiting CSI feedback in the inner and outer closed-loops.

and outer closed-loops. The outer closed-loop system consists of a reconfigurable rateless code [2]. However, in contrast to the work presented in [2], we enhance the achievable performance by appropriately embedding pilots symbols into the generated codeword. The inner closed-loop system is then constituted by a single-user MIMO transmit eigen-beamforming scheme. These two components of Figure 1 are separated by a pilot position interleaver and by an Alamouti space-time block code (STBC) [3]. Furthermore, we assume an error- and delay-free feedback channel having infinite accuracy.

A. Outer Closed-Loop: Encoder for PSAR Codes

For every information bit sequence to be encoded at a specific transmission instant ι, the CSI received via the feedback channel is exploited by what we refer to as the degree distribution selector[1] (DDS) of Figure 1 in order to calculate the required coding rate R_ι as well as the corresponding irregular degree (or check node) distribution $\delta_\iota(x)$. The latter can be conveniently represented by means of a polynomial distribution defined by:

$$\delta_\iota(x) := \delta_1 + \delta_2 x + \ldots + \delta_{d_c} x^{d_c-1} + \ldots + \delta_{D_c} x^{D_c-1}, \qquad (1)$$

where the positive coefficients δ_{d_c}, $d_c \in \mathbf{d}^\iota$ denote the particular fraction of intermediate bits (or check nodes) of degree d_c and $D_c = \max(\mathbf{d}^\iota)$ is the maximal check (left) degree. The vector $\mathbf{d}^\iota$ contains the range of (check) degree values of the degree distribution. In contrast to [2], there is now two different categories of degree-one bits and as a result, the fraction δ_1 of (1) can be rewritten as $\delta_1 = \delta_1^p + \delta_1^{\overline{p}}$, where δ_1^p and $\delta_1^{\overline{p}}$ denote the fraction of degree-one nodes corresponding to pilot bits and to information bits, respectively. The rateless encoder of Figure 1 maps a K-bit (input) information sequence represented by $\mathbf{a} = [a_1, a_2, \ldots, a_K]$ into a $(K^{'} R_\iota^{-1})$-bit output sequence $\mathbf{c}$ by first attaching a predetermined pilot-bit sequence $\mathbf{p} = [p_1, p_2, \ldots, p_{K_p}]$, to the beginning of the K-bit input stream $\mathbf{a}$, so that the modified $K^{'}$-bit input sequence becomes equal to $\mathbf{a}' = [\mathbf{p}\ \mathbf{a}]$. Subsequently, a degree d_c is randomly chosen from the degree distribution $\delta_\iota(x) - \delta_1^p$ calculated by the degree distribution selector based upon the received CSI. Then, the previously selected d_c number of bits are randomly selected from $\mathbf{a}'$ having the least number of connections (selections) up to the current transmission instant.[2] The value of the intermediate (check) bit $b_i \in \mathbf{b}$ is then calculated by combining the d_c input bits selected during the previous step using modulo-2 addition and then repeating the last three steps to all the $K^{'}$ bits of $\mathbf{a}'$. Afterwards, the same pilot bit sequence $\mathbf{p}$ as in the initial step is again attached to the beginning of the intermediate bit sequence $\mathbf{b}$ generated in the previous step in order to create $\mathbf{b}' = [\mathbf{p}\ \mathbf{b}]$. Finally, the value of the encoded bit $c_i \in \mathbf{c}$, $i = 1, \ldots, K^{'} R_\iota^{-1}$ is determined by calculating the values of $c_1 = b_1^{'}$ and of $c_i = b_i^{'} \oplus c_{i-1}$ for $i = 2, \ldots, K^{'} R_\iota^{-1}$, where $b_i^{'} \in \mathbf{b}^{'}$ and $\oplus$ represents the modulo-2 addition operation. The pilot bits in $\mathbf{c}$ correspond to the bits $c_i \in \mathbf{c}$ with $i = 1, \ldots, K_p$.

We also wish to point out the fact that most rateless codes do have a fixed-rate counterpart; in fact, the proposed PSAR codes can be viewed as instances of rateless repeat accumulate (RA) codes [4], that are however interspersing pilot bits with the actual encoded bits. It can also be readily demonstrated that the number of pilot symbols required according to the predetermined pilot overhead δ_1^p is given by $K_p = (K\delta_1^p) / (R_\iota - \delta_1^p)$. The achievable throughput, T_{eff}, measured in bits/second/Hz, which also takes into consideration the power allocated to the pilot symbols, is then given by $T_{\text{eff}} = R_\iota - \delta_1^p$. It also follows that the proposed PSAR codes can realize any code having $R_\iota > \delta_1^p$. This implies that whilst other rateless codes are capable of generating codes having an arbitrarily rate (see [5] and references therein), PSAR codes can only generate codes having rates that are higher than the fraction of pilots δ_1^p in the code. At first glance this might appear to be a limitation, however we note that δ_1^p is selected according to the worst expected fading rate, and hence for slow-fading channels PSAR codes can practically realize codes having any rate. Moreover, it is more power-efficient for the transmitter to opt for no transmission when the channel's SNR is very low instead of transmitting at a very low code-rate.

B. Pilot-Bit Interleaving and Space-Time Block Coding

The codeword $\mathbf{c}$ is then interleaved by the pilot position interleaver Π_p, which will position a pair of pilots every $(\eta - 1)$ data bits, where η denotes the pilot spacing. This process is similar to that described in [6], which represents the effective sampling of the channel's complex-valued envelope at a rate that is higher than the Nyquist rate and thus allowing the receiver to extract the channel attenuation as well as phase rotation estimates for each bit. The data bits are separated by means of a pair of pilot bits (instead of a single pilot), since the channels between the two transmit and two receive antennas have to be estimated. The interleaved codeword $\pi_p(\mathbf{c})$ is then modulated and re-encoded using the rate-one STBC specified by the transmission matrix $\mathbf{G}_2$ [3]. The space-time codeword will be denoted by $\mathbf{C}$.

C. Inner Closed-Loop System: MIMO Transmit Eigen-beamforming

The inner closed-loop system, also depicted in Figure 1, consists of a single-user MIMO system employing two transmit and two

[1]We will be referring to the degree distribution selector located at the transmitter by DDS_T.

[2]This ensures that the variable or information node distribution, $\upsilon_\iota(x)$, is regular, as defined by $\upsilon_\iota(x) := x^{d_\upsilon - 1}$, where d_υ denotes the variable node degree, i.e. the number of times each input bit $a_i^{'} \in \mathbf{a}^{'}$ has been selected. The distribution $\upsilon_\iota(x)$ is calculated by the DDS_T block of Figure 1 by using a similar technique to that used to determine $\delta_\iota(x)$.

receive antennas. Let the channel impulse responses (CIRs) be stored in the (2×2)-element channel matrix $\mathbf{H}$ containing four elements corresponding to an independent and identically-distributed (i.i.d) complex-valued Gaussian distributed random variables having zero mean and unity variance. The transmit eigen-beamforming scheme can be decomposed in three main components [1], consisting of the input-shaping matrix $\mathbf{V_C}$ representing the eigenvectors of the covariance matrix of the encoded codeword $\mathbf{C}$, the beamforming matrix $\mathbf{V_H}$ and the power allocation vector $\mathbf{d} = [d_1\ d_2]$. These three matrices are formulated by $cov(\mathbf{C}) = \mathcal{E}(\mathbf{C}\mathbf{C}^{\mathrm{H}}) = \mathbf{V_C}\mathbf{\Lambda_C}\mathbf{V_C^H}$, where $(\cdot)^{\mathrm{H}}$ denotes the Hermitian operator. The matrix $\mathbf{\Lambda_C} = \mathrm{diag}[\lambda_{\mathbf{C_1}}\ \lambda_{\mathbf{C_1}}]$, where diag[·] has elements in the leading diagonal and $\lambda_{\mathbf{C}_i}$ with $i = [1, 2]$ correspond to the eigenvalues of $\mathbf{C}$. The task of the input-shaping matrix $\mathbf{V_C}$ is to spatially de-correlate the input signal so as to disperse the input energy in the most effective way across the Alamouti space-time codeword.

On the other hand, the beamforming matrix $\mathbf{V_H}$ is the right-hand side (RHS) singular matrix of the MIMO channel matrix $\mathbf{H}$, hence we have $\mathbf{H} = \mathbf{U_H}\mathbf{\Lambda}_{\mathbf{H}}^{\frac{1}{2}}\mathbf{V_H^H}$, where $\mathbf{U_H}$ represents the unitary, left-hand side singular matrix of $\mathbf{H}$, $\mathbf{\Lambda}_{\mathbf{H}}^{\frac{1}{2}} = \mathrm{diag}[\sqrt{\lambda_{\mathbf{H}_1}}\ \sqrt{\lambda_{\mathbf{H}_2}}]$ and $\lambda_{\mathbf{H}_i}$ with $i = [1, 2]$ corresponds to the eigenvalues of the $\mathbf{H}^{\mathrm{H}}\mathbf{H}$. The beamforming matrix $\mathbf{V_H}$ decouples the input signal into spatially orthogonal modes in order to match the eigen-directions of the MIMO channel.

At each transmission instant, a column of the space-time codeword $\mathbf{C}$, will be linearly transformed by the transmit eigen-beamforming matrix $\mathbf{P}$ before transmission, where $\mathbf{P}$ is formulated by $\mathbf{P} = \mathbf{V_C^H}\mathbf{\Lambda_P}\mathbf{V_H}$, having $\mathbf{\Lambda_P} = \mathrm{diag}[\mathbf{d}]$. The total transmission power at every instant is normalized to unity and controlled by the power allocation vector $\mathbf{d}$. Based on the ergodic capacity-optimization criterion, the power is allocated according to the classic waterfilling algorithm. The power allocated for each layer, P_i, is first calculated based on [1]

$$P_i = \left(\mu - \frac{N_0}{\lambda_{\mathbf{H}_i}}\right)\mathbf{1}\left\{\left(\mu - \frac{N_0}{\lambda_{\mathbf{H}_i}}\right) > 0\right\}, \quad \text{for } i = [1, 2], \tag{2}$$

where $\mathbf{1}\{\cdot\}$ denotes the indicator function and μ denotes what is referred to as the water surface level. Furthermore, P_i must satisfy the total power constraint of $\sum_{i=1}^{2} P_i = 1$. After calculating the value of P_i, the value of the corresponding power gain $d_i \in \mathbf{d}$ is given by $d_i = \sqrt{P_i/\lambda_{\mathbf{C}_i}}$, where $\lambda_{\mathbf{C}_i}$ is the corresponding eigenvalue element residing on the leading diagonal. Furthermore, we note that as illustrated in Figure 1, the space-time codeword corresponding to a pair of pilot bits will bypass the transmit eigen-beamforming stage.

D. Receiver and the Feedback Link

We denote the pilot bits received at the first and second antenna on the first and second time-slot by $y_{1,1}$, $y_{1,2}$, $y_{2,1}$ and $y_{2,1}$, respectively. The four pilots bits, periodically occurring every $(\eta-1)$ data bits, are then passed to the channel estimator (please refer to Figure 1), which aid to estimate the corresponding MIMO channel matrix $\widehat{\mathbf{H}}$ having elements of $\widehat{h}_1$, $\widehat{h}_2$, $\widehat{h}_3$ and $\widehat{h}_4$ formulated by $\widehat{h}_1 = \frac{-\sqrt{2}}{2}(y_{1,1} + y_{1,2}), \widehat{h}_2 = \frac{-\sqrt{2}}{2}(y_{2,1} + y_{2,2}), \widehat{h}_3 = \frac{\sqrt{2}}{2}(y_{1,1} - y_{1,2}), \widehat{h}_4 = \frac{\sqrt{2}}{2}(y_{2,1} - y_{2,2})$, where the scaling factor $\sqrt{2}$ results from the normalization of the transmit power to unity, as alluded to in Section III-C. The channel estimates are then up-sampled and interpolated by means of a low-pass interpolator. Armed with this MIMO channel estimate, the received signal is then detected using a soft-input soft-output (SISO) maximum a-posteriori probability (MAP) detector. The detected signal is then de-interleaved using the pilot position interleaver Π_p described in Section III-B, and then passed to the rateless decoder, which estimates the original information bit sequence, i.e. $\widehat{a}$.

The MIMO channel estimate $\widehat{\mathbf{H}}$ is then quantized according to a predetermined finite set of Z quantization levels. The selected quantization level I_z, where $z = 1, \ldots, Z$, is then transmitted by the MS back to the BS over the feedback channel. The BS performs the inverse-quantization by reconstructing $\widehat{\mathbf{H}}$ using the index value I_z received on the feedback channel. Based on the previous observations of the channel at time instant $t_0, t_0 - \eta, \ldots, t_0 - k\eta$, where t_0 denotes the current time instant, the long-term channel predictor (LTCP) predicts the future CIR taps several instances into the future. As further CSI information is received, the LTCP replaces the previously predicted values with the actual received CSI values.

IV. EXIT Chart Functions of PSAR Codes

The rateless decoder for the PSAR codes is effectively constituted from the serial concatenation of two decoders separated by a uniform random interleaver. The inner decoder is the amalgam of a memory-one trellis decoder used for the accumulator (ACC) and of a check node decoder (CND), whilst the outer decoder is a variable node decoder (VND). The convergence behavior of this decoding process can then be analyzed in a similar manner to that used for other iterative decoding processes by means of observing the evolution of the input and output mutual information exchange between the inner and outer decoders in consecutive iterations, which is diagrammatically represented using the semi-analytical tool of EXIT charts [7]. Given the pair of distributions $\upsilon_\iota(x)$ and $\delta_\iota(x)$, we can then proceed to determine the corresponding EXIT curves representing the two EXIT functions of both the inner and outer decoders. The combined EXIT function $I_{E,D\&A\&C}(\cdot)$ of the detector, accumulator and CND can be approximated as in [7] by:

$$I_{E,D\&A\&C}(I_A, I_E, \mathbf{d}^\iota, \psi_{\mathrm{avg}}) \approx \sum_{\forall d_c \in \mathbf{d}^\iota} \Delta_{d_c}^\iota [1 - J\left(\sqrt{(d_c - 1) \cdot [J^{-1}(1 - I_A)]^2 + [J^{-1}(1 - I_E)]^2}\right)], \tag{3}$$

where the function $J(\cdot)$ denotes the mutual information and $I_A := I_{A,CND} = I_{A,D\&A\&C}$ represents the *a-priori* information input of the CND. The extrinsic information accumulator output is then defined by $I_E := I_{E,ACC}\left[I_{A,ACC}(I_{A,CND}, \mathbf{d}^\iota), I_{E,D}(\psi_{\mathrm{avg}})\right]$, where $I_{A,ACC}$ denotes the *a-priori* accumulator information input and $I_{E,D}$ represents the extrinsic information detector output. The parameter $\Delta_{d_c}^\iota$ in (3) corresponds to the specific fraction of edges emanating from the intermediate bits (or check nodes) of degree $d_c \in \mathbf{d}^\iota$ and is given by

$$\Delta_{d_c}^\iota = \delta_{d_c} \cdot \frac{d_c}{d_{\mathrm{c,avg}}}, \tag{4}$$

and the average check node degree $d_{\mathrm{c,avg}}$ is defined by $d_{\mathrm{c,avg}} := \sum_{\forall d_c \in \mathbf{d}^\iota} \delta_{d_c} \cdot d_c$. Then, by substituting $\delta_1 = \delta_1^p + \delta_1^{\overline{p}}$ into (4) for $d_c = 1$, the fraction of edges attributed to the degree-one pilot nodes as well as to the non-pilot check nodes is given by $\Delta_{d_1}^\iota = \left(\delta_1^p + \delta_1^{\overline{p}}\right) / (d_{\mathrm{c,avg}})$.

For the particular case of the proposed PSAR codes (and thus in contrast to [7]), the inner decoder's EXIT function $I_{E,D\&A\&C}(I_A, I_E, \mathbf{d}^\iota, \psi_{\mathrm{avg}})$ can be analyzed in terms of three separate components as follows

$$\begin{aligned} I_{E,D\&A\&C}(\cdot) \approx\ & I^1_{E,D\&A\&C}(I_A, I_E, \psi_{\mathrm{avg}}, \forall d_i \in \mathbf{d}^\iota | i > 1) \\ & + I^2_{E,D\&A\&C}(I_A, I_E, \psi_{\mathrm{avg}}, \forall d_1 \in \mathbf{d}^\iota | \delta_1 = \delta_1^{\overline{p}}) \\ & + I^3_{E,D\&A\&C}(\forall d_1 \in \mathbf{d}^\iota | \delta_1 = \delta_1^p). \end{aligned} \tag{5}$$

The first component of (5) represented by the function $I^1_{E,D\&A\&C}(\cdot)$ is determined by using (3) and by substituting $d_c \in \mathbf{d}^\iota$ for all the check nodes that are higher than one. It may be readily shown that the second and third constituent functions of (5) are then approximated by

$$\begin{aligned} I^2_{E,D\&A\&C}(\cdot) &\approx \frac{\delta_1^{\overline{p}}}{d_{\mathrm{c,avg}}}\left[1 - J\left(\sqrt{[J^{-1}(1-I_E)]^2}\right)\right] \\ &= \frac{\delta_1^{\overline{p}}}{d_{\mathrm{c,avg}}} I_E, \end{aligned} \tag{6}$$

whilst $I^3_{E,D\&A\&C}(\cdot)$ is determined by the multivariable limit formulated by

$$\begin{aligned} I^3_{E,D\&A\&C}(\cdot) \approx & \lim_{(I_A,\psi_{\mathrm{avg}}) \to (1,\infty)} \frac{\delta_1^p}{d_{\mathrm{c,avg}}}\left[1 - J\left(\left[J^{-1}(1-I_E)\right]\right)\right] \\ = & \frac{\delta_1^p}{d_{\mathrm{c,avg}}}. \end{aligned} \tag{7}$$

In (7), we are seeking the limit as $(I_A, \psi_{\mathrm{avg}}) \to (1,\infty)$ since the fraction δ_1^p corresponds to pilot check nodes, which receive perfect messages from both the pilot parity nodes as well as from the pilot variable nodes. Subsequently, we can substitute (5), (6) and (7) into (3), yielding

$$\begin{aligned} I_{E,D\&A\&C}(\cdot) \approx & \frac{1}{d_{\mathrm{c,avg}}}\left(\delta_1^p + \delta_1^{\overline{p}} I_E\right) + \sum_{\forall d_c \in \mathbf{d}^\iota \setminus d_1} \Delta^\iota_{d_c}[1 - \\ & J\left(\sqrt{(d_c-1)\cdot[J^{-1}(1-I_A)]^2 + [J^{-1}(1-I_E)]^2}\right)]. \end{aligned} \tag{8}$$

Given a variable node distribution υ_ι, the outer decoder's EXIT function representing the extrinsic information output of the VND can be formulated in a similar manner to that of a non-systematic RA code [7], namely as $I_{E,VND}(I_{A,VND}, d_v) = J\left[\sqrt{(d_v-1)}\cdot J^{-1}(I_{A,VND})\right]$, where $I_{E,VND}(I_{A,VND}, d_v)$ represents the extrinsic information output of the VND as a function of the its *a-priori* information input $I_{A,VND}$ and its variable node degree d_v.

V. EXIT Chart Based Optimization for PSAR Codes

This section details the technique employed by the degree distribution selectors in order to determine the specific check and variable node distribution, $\delta_\iota(x)$ and $\upsilon_\iota(x)$ that maximizes the achievable code-rate. This optimization problem is tackled by the following linear programming approach, with the primal problem formulated by

$$\max \sum_{\forall d_c \in \mathbf{d}^\iota} \frac{d_c}{\Delta^\iota_{d_c}} \tag{9}$$

subject to the *equality constraint*

$$\sum_{\forall d_c \in \mathbf{d}^\iota} \Delta^\iota_{d_c} = 1 \tag{10}$$

and to the *inequality constraints* given by

$$I_{E,D\&A\&C}(\mathcal{I}, \mathbf{d}^\iota, \psi_{\mathrm{avg}}) > I_{A,VND}(\mathcal{I}, d_v) + \varsigma, \tag{11}$$

and

$$\Delta^\iota_{d_c}|_{\forall d_c \in \mathbf{d}^\iota} > 0, \tag{12}$$

where (10) and (12) ensures that the resultant $\Delta^\iota_{d_c}$ values are both valid and non-negative. The parameter $\mathcal{I}$ represents the discrete set of gradually increasing values in the interval $[0,1]$ over which the functions $I_{E,D\&A\&C}(\cdot)$ and $I_{A,VND}(\cdot) = I^{-1}_{E,VND}(\cdot)$ are calculated, whilst ς assumes values across $\mathcal{I}$, which determines the area of the tunnel between the two EXIT curves. Optimizing the objective function of (9) subject to the above-mentioned constrains, will determine the feasible set of candidate solutions having values of $\Delta^\iota_{d_c}$ (and consequently δ_{d_c}) corresponding to the specific check node degrees $d_c \in \mathbf{d}^\iota$ that substantiate that distribution $\delta_\iota(x)$, which maximizes the design rate, for a predefined d_v value.

Nevertheless, we remark that the constraints represented in (10), (11) and (12) on their own are not sufficient to guarantee that the resultant PSAR code will provide a δ_1^p-fraction of pilot bits. For this particular reason, a stricter constraint than that of (12) must be introduced for the specific fraction of edges $\Delta^\iota_{d_1}$ terminating in degree-one check nodes, which must also obey $\Delta^\iota_{d_1} \geq \delta_1^p / d_{c,avg}$. The difficulty in satisfying the latter constraint arises from the dependence of $\Delta^\iota_{d_1}$ on the average check node degree $d_{c,avg}$, where the latter is again dependent on the value of $d_c \in \mathbf{d}^\iota$ as well as on the value of δ_{d_c}, both of which constitute part of the set of solutions for the optimization problem considered. This problem is circumvented by utilizing a search algorithm, similar to a binary search algorithm, which progressively finds better estimates of the required $\Delta^\iota_{d_1}$ value that results in the required δ_1^p-fraction of pilot bits.

The first step of the PSAR code design technique was that of solving the optimization problem of (9) satisfying the constraints of (10), (11) and (12), and temporarily setting δ_1^p to zero. This initial step is carried out in order to estimate the number of degree one check nodes that are available. The fraction of degree one nodes, δ_1, is then calculated according to (4) and using the $\Delta^\iota_{d_1}$ value resulting from the first run of the linear program.

We will denote the fraction of edges and nodes calculated after the i^{th} evaluation of the objective function of (9) by $\Delta^\iota_{d_1,i}$ and $\delta_{1,i}$, respectively. Following this, if the resultant initial value $\delta_{1,1}$ is smaller than the target value δ_1^p, the linear program is run again by introducing a fourth inequality constraint given by $\Delta^\iota_{d_1} > 2\Delta^\iota_{d_1,1}$. In doing so, the value $\Delta_{d_1,1}$ is set to be the (temporarily) lowest value of the search interval $\Delta^\iota_{d_1}$. After the second iteration, which provides the solution for both $\Delta^\iota_{d_1,2}$ and for the corresponding fraction $\delta_{1,2}$, a comparison is made again between $\delta_{1,2}$ and the target fraction of pilots. If the value of $\delta_{1,2}$ is found to be larger than δ_1^p, the value of $\Delta^\iota_{d_1,2}$ is set to be the (temporarily) highest value of the search interval. The search may then continue by solving the objective function of (9) for the third time, with the additional fourth constraint of $\Delta^\iota_{d_1} > \left(\Delta^\iota_{d_1,2} - \Delta^\iota_{d_1,1}\right)/2$. On the other hand, if the calculated value $\delta_{1,2}$ is again smaller than the target value, the value $\Delta^\iota_{d_1,2}$ becomes the new lowest value of our search interval and the additional fourth constraint is twice this lowest value; i.e. $\Delta^\iota_{d_1} > 2\Delta^\iota_{d_1,2}$. Following this, every further run of the linear program will enable use to narrow our search interval by a factor of two, until the target value is found.

VI. Simulation Results and Concluding Remarks

The results presented in this section were obtained using BPSK modulation, when transmitting over a correlated Rayleigh channel. The proposed rateless codes were decoded using the classic belief propagation (BP) algorithm, in a similar fashion to the decoding of LDPC codes. The rateless decoder was limited to a maximum of $I_{\max}$ = 200 iterations. Three different mobile terminal's velocities were considered; a pedestrian speed of 3 mph, and vehicular speeds of 60 mph as well as of 100 mph. The data signaling rate and the carrier frequency were those from the Universal Mobile Telecommunication System (UMTS) standard, and were set to 15 kbps and 2 GHz, respectively. Figure 2 illustrates the exhibited average throughput performance parameterized with the

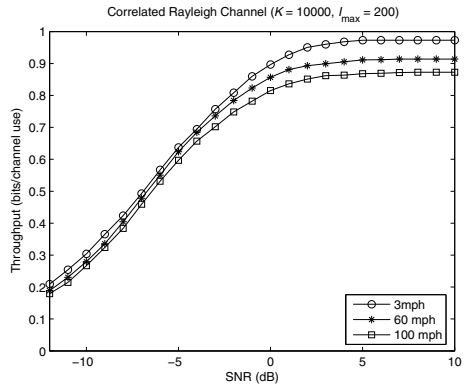

Fig. 2. A comparison of the achievable average throughput performance (measured in bits/channel use) versus the SNR (in dB) for transmission over an correlated Rayleigh channel using BPSK modulation. The number of information bits for the rateless code, K, was set to 10000 bits and the maximum number of decoder iterations, $I_{\max}$ was fixed to 200 iterations. The mobile terminal's velocity was set to 3 mph, 60 mph and 100mph. The fraction of pilot bits, δ_1^p, was set to 0.05 (for the 3 mph and 60 mph scenario) and to 0.1 (for the 100 mph scenario).

mobile terminal velocity, for the range of channel SNR values considered. It can be observed that by increasing the velocity from 3 mph to 100 mph, the throughput performance suffers a loss of approximately 0.1 bits/channel use in the high SNR region. The difference in the throughput performance between the 3 mph and 100 mph scenario in the low-to-medium channel SNR region was about 0.5 dB.

Figure 3 illustrates our comparison of the achievable throughput performance as well as the rateless decoder's computational complexity for both the proposed PSAR code-aided, generalized MIMO transmit preprocessing scheme and for a benchmarker. The benchmarker is the same transmit preprocessing scheme, but instead of having a PSAR code, we use a rateless code dispensing with pilots (i.e. we set $\delta_1^p = 0$ at the encoding stage, which was previously described in Section III-A) but then insert the required number of pilots at the modulation stage. In this sense, we are comparing pilot symbol assisted (rateless) coding with that of pilot symbol assisted modulation in an attempt to verify which of the two techniques offers a better performance (in terms of achievable throughput as well as complexity) for the same amount of pilot overhead. For both systems, the rateless decoder's computational complexity was evaluated in terms of the number of message-passing updates per decoded bit. It can be observed from Figure 3 (top) that there is no difference in the throughput performance of the two systems. On the other hand, the proposed PSAR code-aided system offers a considerable reduction in the rateless decoder's computational complexity, as shown in Figure 3 (bottom).[3] It was found that the complexity reduction in this specific scenario is (on average) more than 30%. Similarly, we have observed a complexity reduction of 25%, when the mobile velocity was reduced from 100 mph to 60 mph. The δ_1^p-fraction of pilot bits was subsequently reduced from 0.1 to 0.05.

In conclusion, we have demonstrated that the PSAR code-aided MIMO transmit preprocessing scheme gleans more benefits from the inserted pilots than the classic PSAM technique, because the pilot bits are not only useful for sounding the channel at the receiver but also beneficial for significantly reducing the computational complexity of the rateless channel decoder. On the other hand, the inevitable energy and throughput loss due to the periodically inserted pilot symbols in the classic PSAM technique is only compensated by the capability of channel estimation.

[3]The fact that our system is only showing a complexity reduction, rather than a throughput performance improvement, was expected due to the specific encoding strategy outlined in Section III-A. Furthermore, we remark that the benchmarker system *has also been optimized* in order to attain the maximum possible achievable throughput at the SNR considered. Additional details can be found in [8], [9].

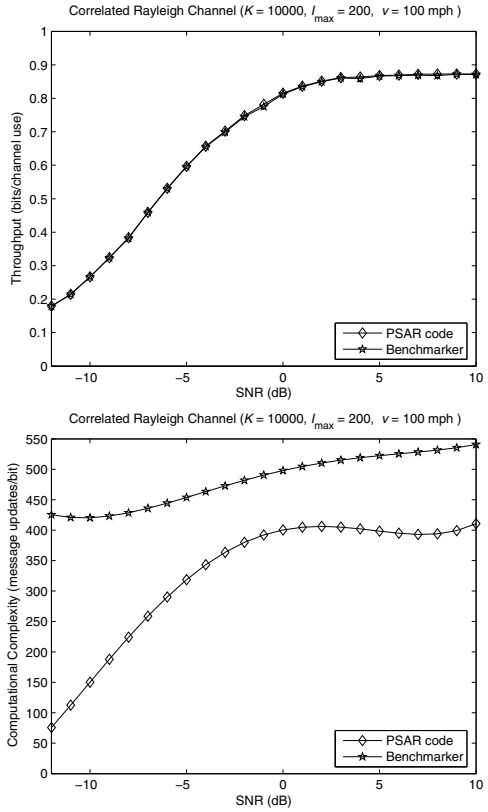

Fig. 3. A comparison of the (a) achievable average throughput performance (measured in bits/channel use) (top figure) and (b) rateless decoder's computational complexity (measured in message updates/bit) of the PSAR code and the benchmarker scenario, versus the SNR (in dB), assuming transmission over an correlated Rayleigh channel using BPSK modulation. The benchmarker scenario consists of a rateless code, which is not aided with pilot symbols (i.e. set $\delta_1^p = 0$), and then followed by PSAM with a 10% pilot overhead. The number of information bits for both scenarios, K, was set to 10000 bits and the maximum number of decoder iterations, $I_{\max}$ was fixed to 200 iterations. The mobile terminal's velocity was set to 100 mph and the fraction of pilot bits for the PSAR code, δ_1^p, was set to 0.1.

REFERENCES

[1] M. Vu and A. Paulraj, "MIMO wireless linear precoding," *IEEE Signal Processing Magazine*, vol. 24, pp. 86–105, Sept. 2007.

[2] N. Bonello, R. Zhang, S. Chen, and L. Hanzo, "Reconfigurable rateless codes," *IEEE Transactions on Wireless Communications*, vol. 8, pp. 5592–5600, Nov. 2009.

[3] S. M. Alamouti, "A simple transmit diversity technique for wireless communications," *IEEE Journal on Selected Areas in Communications*, vol. 16, pp. 1451–1458, Oct. 1998.

[4] H. Jin, A. Khandekar, and R. McEliece, "Irregular repeat-accumulate codes," in *Proceedings* 2nd *International Symposium on Turbo Codes and Related Topics*, (Brest, France), pp. 1–8, Sept. 2000.

[5] N. Bonello, S. Chen, and L. Hanzo, "LDPC codes and their rateless relatives." accepted in the IEEE Communications Surveys and Tutorials.

[6] J. K. Cavers, "An analysis of pilot symbol assisted modulation for Rayleigh faded channels," *IEEE Transactions on Vehicular Technology*, vol. 40, pp. 686–693, Nov. 1991.

[7] S. ten Brink and G. Kramer, "Design of repeat-accumulate codes for iterative detection and decoding," *IEEE Transactions on Signal Processing*, vol. 51, pp. 2764–2772, Nov. 2003.

[8] N. Bonello, S. Chen, and L. Hanzo, "Pilot symbol assisted coding," *Electronics Letters*, vol. 45, pp. 518–519, May 2009.

[9] N. Bonello, D. Yang, S. Chen, and L. Hanzo, "Generalized MIMO transmit preprocessing using pilot symbol assisted rateless codes," *IEEE Transactions on Wireless Communications*, vol. 9, pp. 754–763, Feb. 2010.